# An Evaluation for Iron Contamination in Silicon Solar Cell Using Ideality Factor and Machine Learning

Oleg Olikh, Oleg Lozitsky, and Oleksii Zavhorodnii

***Abstract*—The abstract goes here.**

***Index Terms*—ideality factor, silicon, $n^+$–$p$–$p^+$ structure, SCAPS, iron contamination, machine learning**

## I. Introduction

NON–DESTRUCTIVE methods of evaluation of the impurities contamination in semiconductor crystals and structures, in particular solar cells (SCs), are important from an applied point of view. To date, a not little collection of direct methods (an infrared tomography, an electron-paramagnetic resonance, a non-stationary spectroscopy, etc.) as well as indirect methods (a surface photovoltage, a minority carrier lifetime measurements) has been developed to solve this problem. But almost all of them require special sample preparing or/and specialized equipment. At the same time, the current–voltage curve (IVC) measurement is a widespread method of SC characterization and allows to determine a number of fundamental SC parameters. Evidently SC parameters in particular and the processes of carrier propagation in general depend on electrically active defects presence; therefore there is a possibility in principle to determine the impurity concentration by IVC shape. And recent papers demonstrate a novel approach to extract defect properties from inexpensive IV measurements of completed devices [1].

One of the main obstacles of such a convenient and express method developing is the multiparameter relationship between the contamination of recombination centers and IVC's characteristics, which determined from experimental data. However, in the last decade, the deep learning, which are enable to solve problems without clear algorithmization, have been successfully used in various fields of theoretical and applied physics [2]–[4]. Furthermore, some authors have state that materials informatics (combination of material property calculations/measurements and informatics algorithms) was become the fourth (along with theory, simulations, and experiments) paradigm of science in the past few years [5]. This gives hope for an real implementation of aforesaid SC characterization method with using of deep learning approach (so to say "deep learning for deep levels").

In this work, we use numerical device models to show the possibility of such an approach fulfillment using the example of evaluation the iron concentration in $n^+$–$p$–$p^+$-Si by the ideality factor value. The reasons for aforesaid system consideration are following. Although the ideality factor $n = 2$ is often used to describe the trap related recombination, $n$ value is known to depend on defect parameters, including the concentration [6]–[10]. Consequently the ideality factor is often used to characterize the various semiconductor barrier structures [10]–[14]. We have previously demonstrated [15] the correlation between defect contamination and $n$ value, but the corresponding analytic expressions were not obvious and calibration curves were needed. The iron is a major contaminant as well as one of the most detrimental (and hence, best characterized) metal impurities in silicon photovoltaic devices [1], [16]. A simple back surface field (BSF) $n^+$–$p$–$p^+$ structure is important from an applied point of view.

The deep learning is based on learn by examples. In this work the labeled dataset has been simulated by using SCAPS-1D [17], [18], which was widely used to model silicon-based devices [19]–[21] as well. Obviously, experimental measurements would be preferable, but it is practically impossible to find the necessary thousands of samples with the required parameters.

The work milestone are following (i) the IVC simulation of numerous $n^+$–$p$–$p^+$-Si structure with various parameters for different temperatures; (ii) the fitting of the IVC set according to the two–diode model and the extraction of $n$ value set; (iii) the training of deep neural network (DNN) to estimate an iron–related defect contamination by using SC's base thickness as well as doping level, temperature and ideality factor value; (iv) the DNN testing. Fig. 1 shows a schematic of machine learning based approaches to iron contamination evaluation in which the simulation provides training data. The consequent Sections give the details.

## II. Simulation Details

### A. Temperature Dependencies of Material Parameters

To receive more relevant labeled data, the IVC simulation was performed with regard to following silicon properties:

1) the bandgap temperature dependence according to Pässler equation [22];
2) the doping induced bandgap narrowing [23];
3) the thermal carrier velocities from [24];
4) the temperature dependence of effective states density according to [25];
5) the free carrier effective masses from [26]

The authors are with the Faculty of Physics, Taras Shevchenko National University of Kyiv, 64/13, Volodymyrska Street, City of Kyiv, Ukraine, 01601 (e-mail: olikh@knu.ua).

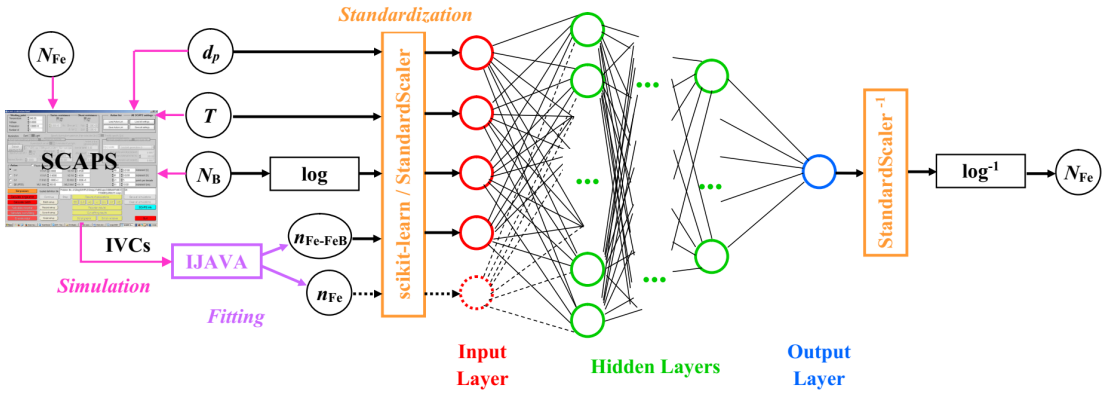


Fig. 1. Flowchart of the work steps. Additional details are discussed in the body of the article.

6) the carrier mobilities according to Klaassen's theory [27];
7) the temperature and doping level dependencies of band–to–band and Auger recombination coefficients from [28] and [29] respectively.

### B. Defect Parameters

The simulation was carried out under the assumption that the defect–assisted recombination was bound up with iron–related deep levels. We have assumed uniform iron atom distribution in both SC base ($p$–region) and BSF–layer ($p^+$–region) with concentration $N_{\mathrm{Fe}}$. Simulations were carried out for two cases. In the first equilibrium one, the iron is believed to be both in the interstitial lattice position ($\mathrm{Fe}_i$) and in the trigonal pair with shallow acceptors (boron, $\mathrm{Fe}_i\mathrm{B}_s$). The pair's fraction does not constant in SC regions and is given by [30], [31]

$$\frac{N_{\mathrm{FeB}}}{N_{\mathrm{Fe}}} = \frac{N_{\mathrm{B}} 10^{-23} \exp\left(-\frac{E_b}{kT}\right)}{\left[1+\frac{N_{\mathrm{B}}}{10^{23}}\exp\left(-\frac{E_b}{kT}\right)\right]\left[1+\exp\left(-\frac{F-E_{\mathrm{Fe}_i}}{kT}\right)\right]}, \quad (1)$$

where $N_{\mathrm{B}}$ is the boron concentration, $F$ is the Fermi level, $E_b = 0.582$ eV is the binding energy of the $\mathrm{Fe}_i\mathrm{B}_s$ pairs, $E_{\mathrm{Fe}_i}$ is the donor level, associated with $\mathrm{Fe}_i$. This case referred as "Fe-FeB" hereafter.

In the second one (referred as "Fe"–case), the $\mathrm{Fe}_i$ was suggested to be only present with uniform distribution. Such state can be realized by heat treatment (210°C, 3 min) [32] or intense illumination [33].

The donor level $E_{\mathrm{Fe}_i} = E_V + 0.394$ eV with electron $\sigma_{n,\mathrm{Fe}} = 3.47\times10^{-11}T^{-1.48}$ cm$^2$ and hole $\sigma_{p,\mathrm{Fe}} = 4.54\times10^{-16}\exp\left(-\frac{0.05}{kT}\right)$ cm$^2$ capture cross-sections [30], [34] was associated with $\mathrm{Fe}_i$. The donor level $E^{\mathrm{D}}_{\mathrm{FeB}} = E_V + 0.10$ eV, $\sigma^{\mathrm{D}}_{n,\mathrm{FeB}} = 4\times10^{-13}$ cm$^2$, $\sigma^{\mathrm{D}}_{p,\mathrm{FeB}} = 2\times10^{-14}$ cm$^2$ and acceptor level $E^{\mathrm{A}}_{\mathrm{FeB}} = E_C - 0.26$ eV, $\sigma^{\mathrm{A}}_{n,\mathrm{FeB}} = 5.1\times10^{-9}T^{-2.5}$ cm$^2$, $\sigma^{\mathrm{A}}_{p,\mathrm{FeB}} = 3.32\times10^{-10}\exp\left(-\frac{0.262}{kT}\right)$ cm$^2$ [30], [34], [35] were used in simulation for $\mathrm{Fe}_i\mathrm{B}_s$.

### C. Structure Parameters

The dark IVCs for $n^+$–$p$–$p^+$-Si structure were simulated. The thickness and donor concentration for emitter layer ($n^+$) were 0.5 $\mu$m and $10^{19}$ cm$^{-3}$. The BSF–layer with thickness 1 $\mu$m and acceptor concentration $5\times10^{18}$ cm$^{-3}$ was used. The base thickness $d_p$ (150–240 $\mu$m) and doping level (boron concentration, $N_{\mathrm{B}} = 10^{15}$–$10^{17}$ cm$^{-3}$) changed from one simulation to another. Other varied parameters were temperature ($T = 290$–$340$ K) and iron concentration ($N_{\mathrm{Fe}} = 10^{10}$–$10^{13}$ cm$^{-3}$).

4 $d_p$ values, 9 $N_{\mathrm{B}}$ values, 11 $T$ values and 19 $N_{\mathrm{Fe}}$ values, which evenly (for $T$ and $d_p$ in linear scale, for $N_{\mathrm{Fe}}$ and $N_{\mathrm{B}}$ in logarithmic scale) distributed over the above ranges, formed a kind of parameter's grid. To obtain training dataset, 15048 IVCs were simulated in Fe-case and Fe-FeB-case for nodes of grid.

Besides IVCs were prepared for several test datasets as well. For example, one IVCs set was simulated by using $d_p$, $N_{\mathrm{Fe}}$ and $N_{\mathrm{B}}$ values from grid nodes and divergent $T$ values. The corresponding test dataset is labeled "T-varied" from now on. The value of $d_p$, $N_{\mathrm{Fe}}$ and $N_{\mathrm{B}}$ are divergent from grig in "d-varied", "Fe-varied" and "B-varied" dataset, respectively. "All-varied" dataset was calculated with using all parameter values, unmatched to ones of training dataset. The precise parameters values are listed in Supplementary Material.

### D. Ideality factor determination

The simulated IVCs were fitted by using double diode model [36] equation with neglecting of both series and shunt resistances:

$$I = I_{01}\left[\exp\left(-\frac{qV}{kT}\right)-1\right] + I_{02}\left[\exp\left(-\frac{qV}{nkT}\right)-1\right], \quad (2)$$

where $I_{01}$ and $I_{02}$ are the saturation currents. The fitting was performed by using the meta–heuristic method IJAVA [37].

The ideality factor value $n_{\mathrm{Fe}}$ and $n_{\mathrm{Fe-FeB}}$ corresponds to Fe-case and Fe-FeB-case respectively. The typical simulated dependencies of the ideality factor are shown in Fig. 2. It should be noted that $n$ can takes equal values for different parameters values and dependencies of $n_{\mathrm{Fe}}$ and $n_{\mathrm{Fe-FeB}}$ are slightly vary. The discussion about $n_{\mathrm{Fe}}$ and $n_{\mathrm{Fe-FeB}}$ values are presented elsewhere [38].

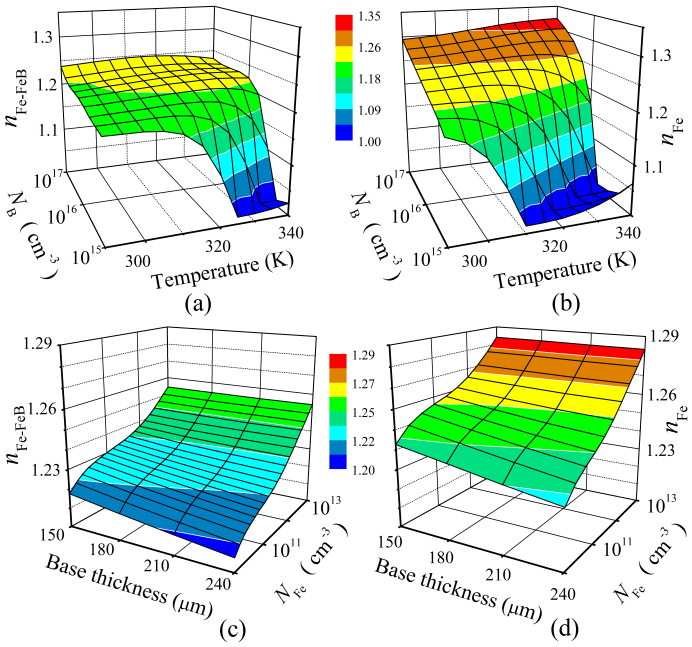


Fig. 2. Ideality factor as a function of the temperature and boron concentration (a, b) or the base thickness and iron concentration (c,d). The cases of $Fe_iB_s$ and $Fe_i$ coexistence (a, c) and interstitial iron presence only (b, d). $N_{\rm Fe} = 10^{10}$ cm$^{-3}$ (a,b), $d_p = 180$ $\mu$m (a, b), $N_{\rm B} = 10^{16}$ cm$^{-3}$ (c, d), $T = 320$ K (c, d).

## III. Results of deep neural network using

We have tried to construct the DNN, which is able to estimate iron contamination by using SC parameters ($d_p$ and $N_{\rm B}$) and results of IVC fitting (ideality factor value) taking into account the measurement temperature. In one case, the result of only one dark IV measurement was used and the set of DNN input parameters (one DNN–sample) consisted of $\{d_p, N_{\rm B}, T, n_{\rm Fe-FeB}\}$. Such case can be easy realized in practice and corresponding neural network referred as $n_{\rm Fe-FeB}$ DNN hereafter. In another case the set $\{d_p, N_{\rm B}, T, n_{\rm Fe-FeB}, n_{\rm Fe}\}$ was used in DNN input. In practice terms, the obtaining of such a set requires additional SC processing (e.g. intense illumination) and two IV measuring. The label $n_{\rm Fe-FeB}$–$n_{\rm Fe}$ DNN is used below.

The DNN's flowchart is shown on Fig. 1. The Keras API [39] was used to set up DNN with dense layers. Four hidden layers with 300, 100, 30 and 30 nodes were selected. The activation function was chosen to be Relu. The learning rate, batch size and number of epochs were kept at 0.01, 8 and 1000 respectively. $\log N_{\rm B}$ and $\log N_{\rm Fe}$ were used instead $N_{\rm B}$ and $N_{\rm Fe}$ in DNN training and testing. Standardization of a dataset was done by using *StandardScaler* from *scikit-learn* (mean $= 0$, standard deviation $= 1$). The loss function was chosen mean square relative error (MSRE):

$$MSRE = \frac{1}{N_s}\sum_{i=1}^{N_s}\frac{(N_{\rm Fe,TRUE,i} - N_{\rm Fe,PRED,i})^2}{N_{\rm Fe,TRUE,i}\cdot N_{\rm Fe,PRED,i}}, \quad (3)$$

where $N_s$ is the number of samples in dataset, $N_{\rm Fe,TRUE,i}$ is the iron concentration, which used for simulation of $i$–th sample, $N_{\rm Fe,PRED,i}$ is the DNN prediction for $i$–th sample.

TABLE I
Results of 10–Fold Cross–Validation Of Used DNN

| Dataset | $n_{\rm Fe-FeB}$ DNN | $n_{\rm Fe-FeB}$–$n_{\rm Fe}$ DNN |
|---|---|---|
| training | $0.29 \pm 0.07$ | $0.09 \pm 0.04$ |
| training+test | $0.30 \pm 0.08$ | $0.05 \pm 0.02$ |

TABLE II
A Mean Square Relative Error Of DNN, Learnt by Training Dataset, on Test Dataset

| Dataset | $n_{\rm Fe-FeB}$ DNN | $n_{\rm Fe-FeB}$–$n_{\rm Fe}$ DNN |
|---|---|---|
| T–varied | 0.46 | 0.06 |
| B–varied | 1.2 | 0.25 |
| d–varied | 0.36 | 0.06 |
| Fe–varied | 0.06 | 0.03 |
| All–varied | 0.49 | 0.10 |

10-fold cross-validation

Flowchart of the wafer processing steps for the silicon lifetime protection experiment.

Flow diagram of the ADALINE neuron used for demonstration of light source identication. Additional details are discussed in the body of the article.

FIG. 2. A schematic of machine learning based approaches to likelihood-free inference in which the simulation provides training data for a neural network that is subsequently used as a surrogate for the intractable likelihood during inference. Illustrations of the methods discussed in the text.

The results on IVC simulation, $n_{\rm Fe}$ and $n_{\rm Fe-FeB}$ values and trained DNN are presented at https://github.com/olegolikh/IVcharacteristics.git.

## IV. Conclusion

The conclusion goes here.

## Acknowledgment

The work was supported by National Research Foundation of Ukraine by the state budget finance (project 2020.02/0036 "Development of physical base of both acoustically controlled modification and machine learning–oriented characterization for silicon solar cells")

## References

[1] R. C. Kurchin, J. R. Poindexter, V. Vhnissi, H. Savin, C. del Caizo, and T. Buonassisi, "How much physics is in a currentvoltage curve? inferring defect properties from photovoltaic device measurements," *IEEE J. Photovolt.*, vol. 10, no. 6, pp. 1532–1537, Nov 2020.

[2] G. Carleo, I. Cirac, K. Cranmer, L. Daudet, M. Schuld, N. Tishby, L. Vogt-Maranto, and L. Zdeborová, "Machine learning and the physical sciences," *Rev. Mod. Phys.*, vol. 91, p. 045002, Dec 2019.

[3] S. Ju, S. Shimizu, and J. Shiomi, "Designing thermal functional materials by coupling thermal transport calculations and machine learning," *J. Appl. Phys.*, vol. 128, no. 16, p. 161102, Oct 2020.

[4] S. Rodrigues, H. G. Ramos, and F. Morgado-Dias, "Machine learning pv system performance analyser," *Prog. Photovoltaics Res. Appl.*, vol. 26, no. 8, pp. 675–687, Aug 2018.

[5] S. Ju, S. Shimizu, and J. Shiomi, "Designing thermal functional materials by coupling thermal transport calculations and machine learning," *J. Appl. Phys.*, vol. 128, no. 16, p. 161102, Oct 2020.

[6] J. Beier and B. Voss, "Humps in dark I–V–curves–analysis and explanation," in *Conference Record of the Twenty Third IEEE Photovoltaic Specialists Conference - 1993 (Cat. No.93CH3283-9)*, May 1993, pp. 321–326.

[7] K. McIntosh, P. Altermatt, and G. Heiser, "Depletion–region recombination in silicon solar cells. when does $mdr = 2$?" in *16th European Photovoltaic Solar Energy Conference: Proceedings of the International Conference and Exhibition*. Publisher:James and James (Science Publishers) Ltd, 2000, pp. 250–253.

[8] A. Kaminski, J. J. Marchand, H. El Omari, A. Laugier, Q. N. Le, and D. Sarti, "Conduction processes in silicon solar cells," in *Conference Record of the Twenty Fifth IEEE Photovoltaic Specialists Conference – 1996*, May 1996, pp. 573–576.

[9] Z. Hameiri, K. McIntosh, and G. Xu, "Evaluation of recombination processes using the local ideality factor of carrier lifetime measurements," *Sol. Energy Mater. Sol. Cells*, vol. 117, pp. 251–258, Oct 2013.

[10] A. S. H. van der Heide, A. Schonecker, J. H. Bultman, and W. C. Sinke, "Explanation of high solar cell diode factors by nonuniform contact resistance," *Progress in Photovoltaics: Research and Applications*, vol. 13, no. 1, pp. 3–16, Jan 2005.

[11] L. Duan, H. Yi, C. Xu, M. B. Upama, M. A. Mahmud, D. Wang, F. H. Shabab, and A. Uddin, "Relationship between the diode ideality factor and the carrier recombination resistance in organic solar cells," *IEEE Journal of Photovoltaics*, vol. 8, no. 6, pp. 1701–1709, Nov 2018.

[12] J. Chen, M. Zhu, X. Lu, and X. Zou, "Electrical characterization of gan schottky barrier diode at cryogenic temperatures," *Appl. Phys. Lett.*, vol. 116, no. 6, p. 062102, Feb 2020.

[13] P. Dalapati, N. Manik, and A. Basu, "Analysis of the temperature dependence of diode ideality factor in ingan-based uv-a light-emitting diode," *Semiconductors*, vol. 54, no. 10, pp. 1284–1289, Oct 2020.

[14] P. Calado, D. Burkitt, J. Yao, J. Troughton, T. M. Watson, M. J. Carnie, A. M. Telford, B. C. O'Regan, J. Nelson, and P. R. Barnes, "Identifying dominant recombination mechanisms in perovskite solar cells by measuring the transient ideality factor," *Phys. Rev. Applied*, vol. 11, p. 044005, Apr 2019.

[15] O. Olikh, "Relationship between the ideality factor and the iron concentration in silicon solar cells," *Superlattices Microstruct.*, vol. 136, p. 106309, Dec 2019.

[16] J. Schmidt, "Effect of dissociation of iron–boron pairs in crystalline silicon on solar cell properties," *Progress in Photovoltaics: Research and Applications*, vol. 13, no. 4, pp. 325–331, Jun 2005.

[17] M. Burgelman, P. Nollet, and S. Degrave, "Modelling polycrystalline semiconductor solar cells," *Thin Solid Films*, vol. 361–362, pp. 527–532, Feb 2000.

[18] K. Decock, S. Khelifi, and M. Burgelman, "Modelling multivalent defects in thin film solar cells," *Thin Solid Films*, vol. 519, no. 21, pp. 7481–7484, Aug 2011.

[19] E. Hu, G. Yue, R. Zhang, Y. Zheng, L. Chen, and S. Wang, "Numerical simulations of multilevel impurity photovoltaic effect in the sulfur doped crystalline silicon," *Renewable Energy*, vol. 77, pp. 442–446, May 2015.

[20] A. Hamache, N. Sengouga, A. Meftah, and M. Henini, "Modeling the effect of 1 MeV electron irradiation on the performance of $n^+$–p–$p^+$ silicon space solar cells," *Radiat. Phys. Chem.*, vol. 123, pp. 103–108, Jun 2016.

[21] K. Kim, J. Gwak, S. K. Ahn, Y.-J. Eo, J. H. Park, J.-S. Cho, M. G. Kang, H.-E. Song, and J. H. Yun, "Simulations of chalcopyrite/c-si tandem cells using scaps-1d," *Sol. Energy*, vol. 145, pp. 52–58, 2017.

[22] R. Pässler, "Dispersion-related description of temperature dependencies of band gaps in semiconductors," *Phys. Rev. B*, vol. 66, p. 085201, Aug 2002.

[23] D. Yan and A. Cuevas, "Empirical determination of the energy band gap narrowing in $p^+$ silicon heavily doped with boron," *J. Appl. Phys.*, vol. 116, no. 19, p. 194505, Nov 2014.

[24] M. A. Green, "Intrinsic concentration, effective densities of states, and effective mass in silicon," *J. Appl. Phys.*, vol. 67, no. 6, pp. 2944–2954, Mar 1990.

[25] R. Couderc, M. Amara, and M. Lemiti, "Reassessment of the intrinsic carrier density temperature dependence in crystalline silicon," *J. Appl. Phys.*, vol. 115, no. 9, p. 093705, Mar 2014.

[26] W. O'Mara, R. Herring, and L. Hant, *Handbook of semiconductor silicon technology*. New Jersey, USA: Noyes Publications, 1990.

[27] D. Klaassen, "A unified mobility model for device simulation — I. model equations and concentration dependence," *Solid-State Electron.*, vol. 35, no. 7, pp. 953– 959, Jul 1992.

[28] H. T. Nguyen, S. C. Baker-Finch, and D. Macdonald, "Temperature dependence of the radiative recombination coefficient in crystalline silicon from spectral photoluminescence," *Appl. Phys. Lett.*, vol. 104, no. 11, p. 112105, Mar 2014.

[29] P. P. Altermatt, J. Schmidt, G. Heiser, and A. G. Aberle, "Assessment and parameterisation of Coulomb–enhanced Auger recombination coefficients in lowly injected crystalline silicon," *J. Appl. Phys.*, vol. 82, no. 10, pp. 4938–4944, Nov 1997.

[30] J. D. Murphy, K. Bothe, M. Olmo, V. V. Voronkov, and R. J. Falster, "The effect of oxide precipitates on minority carrier lifetime in p–type silicon," *J. Appl. Phys.*, vol. 110, no. 5, p. 053713, Sep 2011.

[31] W. Wijaranakula, "The reaction kinetics of iron–boron pair formation and dissociation in p–type silicon," *J. Electrochem. Soc.*, vol. 140, no. 1, pp. 275–281, Jan 1993.

[32] G. Zoth and W. Bergholz, "A fast, preperetion-free method to detect irpn in silicon," *J. Appl. Phys.*, vol. 67, no. 11, pp. 6764–6771, Jun 1990.

[33] L. J. Geerligs and D. Macdonald, "Dynamics of light-induced feb pair dissociation in crystalline silicon," *Appl. Phys. Lett.*, vol. 85, no. 22, pp. 5227–5229, Nov 2004.

[34] F. E. Rougieux, C. Sun, and D. Macdonald, "Determining the charge states and capture mechanisms of defects in silicon through accurate recombination analyses: A review," *Solar Energy Materials and Solar Cells*, vol. 187, pp. 263 – 272, Dec 2018.

[35] A. A. Istratov, H. Hieslmair, and E. Weber, "Iron and its complexes in silicon," *Applied Physics A: Materials Science & Processing*, vol. 69, no. 1, pp. 13–44, Jul 1999.

[36] O. Breitenstein, "Understanding the current-voltage characteristics of industrial crystalline silicon solar cells by considering inhomogeneous current distributions," *Opto–Electronics Review*, vol. 21, no. 3, pp. 259–282, Sep 2013.

[37] K. Yu, J. Liang, B. Qu, X. Chen, and H. Wang, "Parameters identification of photovoltaic models using an improved JAYA optimization algorithm," *Energy Conversion and Management*, vol. 150, pp. 742–753, Oct 2017.

[38] O. Y. Olikh and O. V. Zavhorodnii, "Modeling of ideality factor value in $n^+$–$p$–$p^+$–si structure," *Journal of Physical Studies*, vol. 24, no. 4, p. 4701, 2020.

[39] F. Chollet, *Deep Learning with Python*, 2nd ed. Manning, 2017.

**Oleg Olikh** was born in Kyiv, Ukraine, in 1974. He received the Ph.D. (2001) and D.Sc. (2018) in solid state physics from Taras Shevchenko National University of Kyiv. Since 2001, he has been an associate professor in the Department of General Physics at Taras Shevchenko National University of Kyiv. His research interests in semiconductor physics have focused on external (radiation, ultrasound) influence on properties of semiconductor devices.

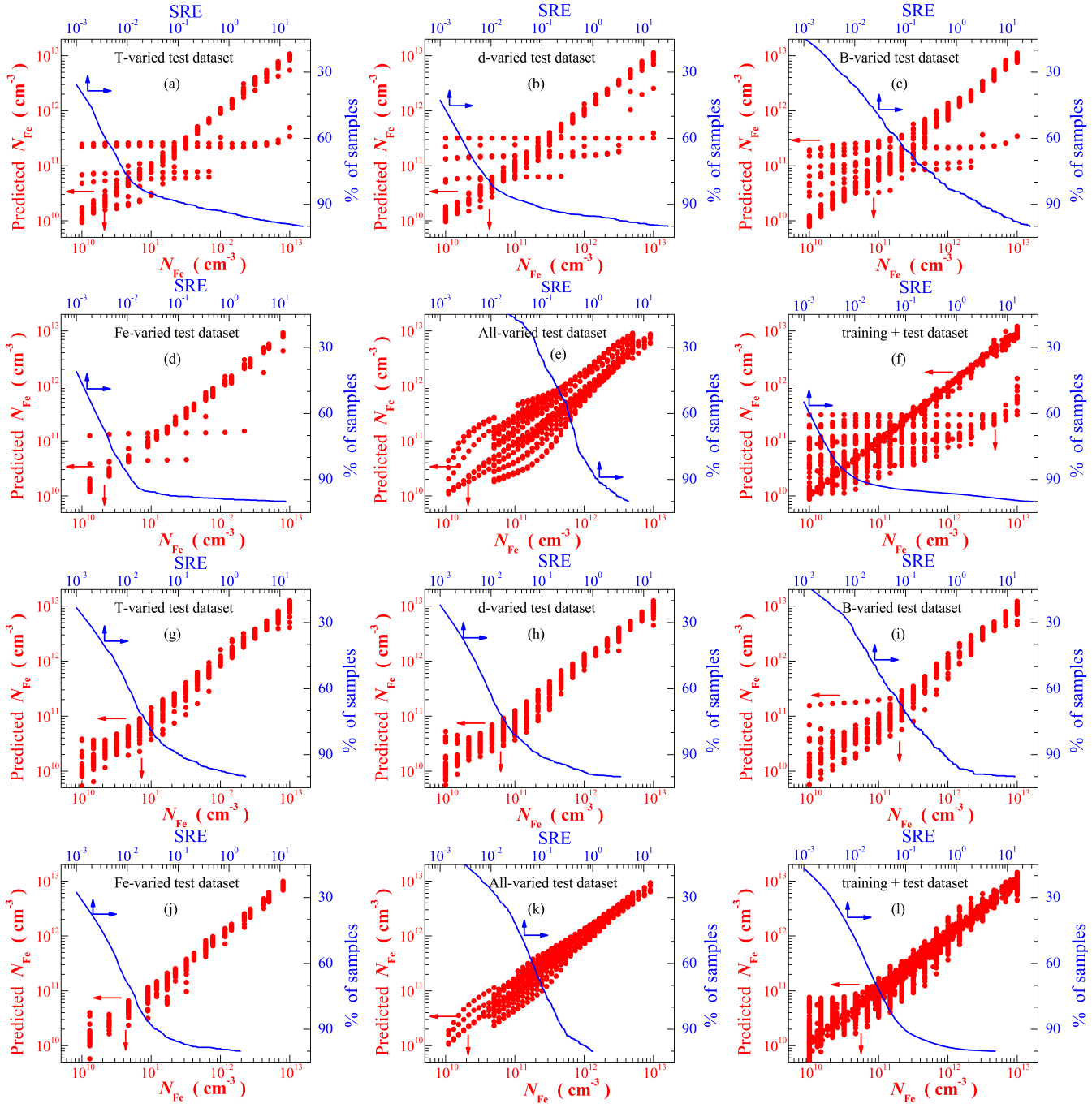


Fig. 3. Comparison of iron contamination retrieval results (red points) and part of samples for which the SRE does not exceed a certain value (blue lines). $n_{\mathrm{Fe-FeB}}$ DNN and $n_{\mathrm{Fe-FeB}}$–$n_{\mathrm{Fe}}$ DNN, learnt by training dataset, are used in panels (a)–(e) and (g)–(k), respectively. Test dataset: T-varied (a, g), d-varied (b, h), B-varied (c, i), Fe-varied (d, j), All-varied (e, k). Panels (f) and (l) represent data from $n_{\mathrm{Fe-FeB}}$ DNN and $n_{\mathrm{Fe-FeB}}$–$n_{\mathrm{Fe}}$ DNN, which learnt by training+test dataset, on the same dataset.